Int. J. Electrochem. Sci., 10 **(2015)** 10132 - 10144

International Journal of
ELECTROCHEMICAL
SCIENCE
www.electrochemsci.org

Electrochemical Na-Insertion/Extraction Properties of Phosphorus Electrodes in Ionic Liquid Electrolytes

Masahiro Shimizu[1,2], *Hiroyuki Usui*[1,2], *Kazuya Yamane*[1,2], *Takuma Sakata*[1,2], *Toshiki Nokami*[1,2], *Toshiyuki Itoh*[1,2], *and Hiroki Sakaguchi*[1,2,*]

[1] Department of Chemistry and Biotechnology, Graduate School of Engineering, Tottori University, 4-101 Minami, Koyama-cho, Tottori 680-8552, Japan
[2] Center for Research on Green Sustainable Chemistry, Tottori University, 4-101 Minami, Koyama-cho, Tottori 680-8552, Japan
[*]E-mail: sakaguch@chem.tottori-u.ac.jp

Received: 26 August 2015 / *Accepted:* 9 September 2015 / *Published:* 4 November 2015

The electrochemical Na-insertion/extraction properties of phosphorus as a Na-ion battery anode in ionic liquid electrolytes were investigated by using a thick film without any binder or conductive additive. The ionic liquid with more electrochemically-stable cation structure, 1-((2-methoxyethoxy)methyl)-1-methylpyrrolidinium bis(fluorosulfonyl)amide (Py1MEM-FSA), delivered a high reversible capacity of 310 mA h g^{-1} at the 100th cycle, whereas the phosphorus electrode in 1-ethyl-3-methylimidazolium bis(fluorosulfonyl)amide (EMI-FSA) showed a low capacity of only 110 mA h g^{-1}. It was revealed that disintegration of the electrode after cycling was effectively suppressed by applying Py1MEM-FSA instead of an organic electrolyte including propylene carbonate (PC), and that a surface layer induced by the decomposition of EMI-FSA hindered Na-insertion into the active material layer. The performance obtained in Py1MEM-FSA was very superior to that in PC. We applied for the first time a closed-system fire-resistance test to the ionic liquid electrolyte for quantitatively evaluating its non-flammability. The Py1MEM-FSA-based electrolyte exhibited an excellent fire resistance in comparison with the PC-based organic electrolyte, which can be an advantage for realizing a Na-ion battery with a high-energy density and a high safety.

Keywords: Phosphorus; Na-ion battery; Thick-film electrode; Ionic liquid electrolyte; Gas deposition

1. INTRODUCTION

Na-ion battery (NIB) is a promising candidate as one of the next-generation energy storage devices due to its low cost and widespread availability of sodium resources [1,2]. Despite the growing interests in NIB, an issue involving the development of high-capacity Na-storage anode materials to be

solved remains to further increase the energy density of the battery. Black phosphorus has attracted much attention as an anode material because of its high theoretical capacity of 2596 mA h g^{-1} [3−5]. The theoretical capacity is about ten times larger than that of carbon-based materials [6−8], and is the highest value in previously-reported active materials such as Sn (847 mA h g^{-1}) [9,10], Sb (660 mA h g^{-1}) [11−13], and Pb (485 mA h g^{-1}) [14]. Although phosphorus can absorb three sodium atoms by a formation of a binary Na−P compound, the volumetric change ratio per phosphorus atom from P to Na_3P (fully sodiated phosphorus) corresponds to 490%, which results in the generation of high stresses and large strains in the active material. The accumulated strains cause disintegration of the phosphorus electrode, leading to a rapid capacity fading. Dou *et al*. reported that the cycling stability of a phosphorus electrode was improved using a carbon nanotube composite; a reversible capacity of 750 mA h g^{-1} was maintained after the 20th charge−discharge cycling [5].

Meanwhile, an electrolyte is one of the most important factors which significantly influences electrode performances. In other words, the choice of electrolyte determines the fate of battery performance. Room-temperature ionic liquids are being intensively investigated as an electrolyte solvent for rechargeable batteries and electrochemical capacitors [15−17]. These studies are motivated by their excellent physicochemical properties of high ionic conductivity, wide electrochemical window, and non-flammability. Among these properties, the nature of non-flammability is quite beneficial for the establishment of non-flammable batteries [18,19]. In the field of Li-ion batteries, our group has demonstrated that the cycling performances of Si-based electrodes are significantly improved by applying an ionic liquid to an electrolyte solvent [20−23]. Furthermore, it was found that the introduction of an ether functional group into cation structure of ionic liquid effectively allows the potential high-capacity of elemental Si. [22]. There has been, however, no study that tried to improve anode performances of phosphorus electrode by utilizing ionic liquid electrolytes to the best of the authors' knowledge. In the present study, therefore, we investigated charge−discharge properties of phosphorus electrode in room-temperature ionic liquids through the use of a thick film prepared by a gas-deposition (GD) method. In order to exactly understand an electrochemical reaction of phosphorus with Na, it is essential to carry out the electrochemical evaluation without any conductive additive or binder typically used in the general preparation of electrodes. The GD method has several advantages as follows: (1) the strong adhesion between the active material particles, as well as between the particles and the substrate, and (2) the nearly unchanged composition in a thick film formed without atomization of the raw material powder [24,25]. These characteristics assist in understanding the electrochemical behavior of phosphorus in ionic liquid electrolytes. We herein report the applicability of ionic liquid electrolytes to a phosphorus electrode for the first time.

2. EXPERIMENTAL

Propylene carbonate (PC; $C_4H_6O_3$, Kishida Chemical Co., Ltd.) as an organic solvent and the ionic liquid of 1-ethyl-3-methylimidazolium bis(fluorosulfonyl)amide (EMI-FSA; KANTO CHEMICAL Co., Inc.) were purchased and used without further purification. 1-((2-methoxyethoxy)methyl)-1-methylpyrrolidinium bis(fluorosulfonyl)amide (Py1MEM-FSA) was

synthesized by an organic method as previously reported [26]. The ionic liquids were dried in a vacuum chamber at 363 K for 24 h for removing water in advance of use. The water content of the ionic liquid was confirmed to be less than 50 ppm using a Karl-Fisher moisture titrator (Labconco Corporation, FZ-Compact). The electrolytes were prepared by dissolving the salt of sodium bis(trifluoromethanesulfonyl)amide (NaTFSA, Kishida Chemical Co., Ltd.) in each solvent at a concentration of 1.0 mol dm^{-3} (M). The electrical conductivities of the electrolytes were measured by an electrochemical impedance instrument (CompactStat, Ivium Technologies) through the use of a cell equipped with two Pt electrodes under an argon atmosphere at various temperatures from 293 to 353 K. Fire-resistance tests for the organic and ionic liquid electrolytes were conducted by using a flash point tester (Setaflash Series: 33000-0, STANHOPE SETA LTD.). These tests were performed in line with the prescribed conditions (*Rapid equilibrium closed cup method* / International Organization for Standardization: ISO 3679:2004 and Japanese Industrial Standards: JIS K2265-2) by ISO [27] and JIS [28] Committee. First, an electrolyte sample of 4 mL was injected into a cup then sealed by an O-ring to avoid volatilization. After the sample cup was heated to the set temperatures and kept at the constant temperatures for two minutes, a test jet flame with a diameter of 4 mm was dipped into the vapor space inside the sample cup from an aperture for a period of 2.5 seconds. At that moment, a flash detector distinguishes the presence or absence of an ignition to evaluate the fire resistance of the samples.

Black-phosphorus powder was simply prepared by a mechanical milling (MM) method using a high-energy planetary ball mill (Classic Line P-6, FRITSCH) in an argon atmosphere. Red-phosphorus powder (Wako Pure Chemical Industries, Ltd., 98.0%) as the starting material (2.4 g) was put in a stainless steel pot together with five stainless steel balls. The weight ratio of the balls to the red-phosphorus powder was 30:1. The MM time and rotation speed were 10 h and 380 rpm, respectively. The crystal structures and Raman spectra of the phosphorus powders were investigated using X-ray diffractometer (Ultima IV Rigaku Co., Ltd.) with CuK_{α} radiation and Raman microscopy system (NanofinderFLEX, Tokyo Instruments, Inc.) with the 532 nm line of a Nd:YAG laser. Phosphorus thick-films were prepared on Cu foil substrates by gas deposition using the resulting phosphorus powder and a helium carrier gas. Further detailed conditions have been described in our previous reports [25,29]. We fabricated 2032-type coin cells consisting of a phosphorus thick-film electrode as the working electrode, Na foil as the counter electrode, electrolyte, and propylene-based separator. Galvanostatic charge−discharge tests were carried out using an electrochemical measurement system (HJ-1001 SD8, Hokuto Denko Co., Ltd.) in the potential range between 0.005 and 2.000 V vs. Na/Na^{+} at 303 K. The current density was 50 mA g^{-1}, corresponding to a *C*-rate of 0.02 *C*. All operations including preparation of electrolytes, active material, thick-film electrodes and cell assembly were performed in a custom-made purge-type glove box (Miwa MFG, DBO-2.5LNKP-TS) filled with an argon atmosphere from which oxygen and water were completely removed. The glove box maintained a dew point below −100 ^{o}C and oxygen content below 1 ppm. The surface morphologies of the phosphorus electrodes after the charge−discharge cycling were observed by a field-emission scanning electron microscope (FE-SEM, JSM-6701F JEOL Co., Ltd.).

3. RESULTS AND DISCUSSION

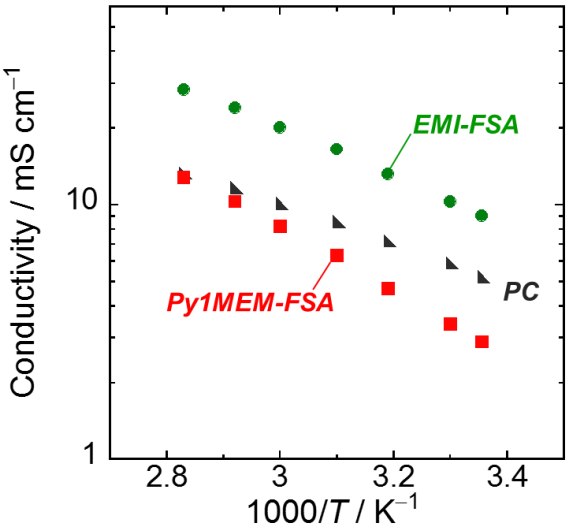

Figure 1. Temperature dependence of conductivity for electrolytes at a concentration of 1.0 M. The measurements were conducted in the range from 298 K to 353 K. The electrical conductivities in PC, Py1MEM-FSA, and EMI-FSA at 303 K are 5.9, 3.4, and 10.3 mS cm^{-1}, respectively.

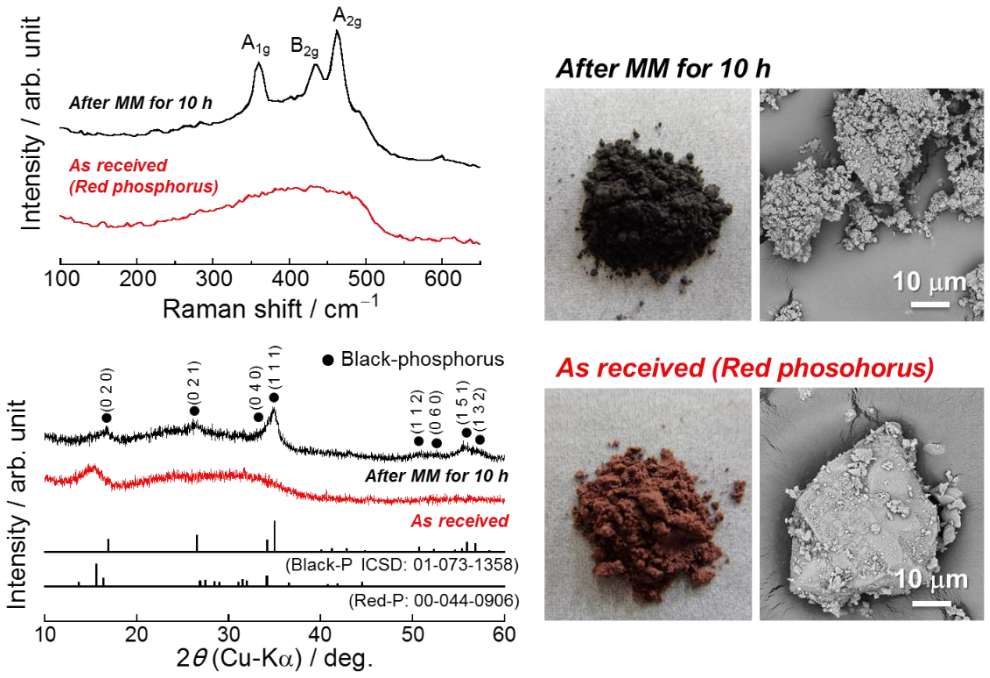

Figure 2. Raman spectra, XRD patterns, photographs, and FE-SEM images of red-phosphorus powder and ball-milled phosphorus powder.

Figure 1 shows temperature dependence of conductivities for various electrolytes at a concentration of 1.0 M. The electrical conductivities of NaTFSA/PC, NaTFSA/Py1MEM-FSA, and NaTFSA/EMI-FSA at 303 K were 5.9, 3.4, and 10.3 mS cm^{-1}, respectively. The EMI-FSA electrolytes

exhibited a higher conductivity than that in Py1MEM-FSA, which means the high ability of ionic transport in the electrolyte solution. As the positive charge in the EMI cation is non-localized, the electrostatic interaction between the EMI cation and FSA anion is weaker in comparison to that consisting of a quaternary ammonium cation and FSA anion. The charge delocalization consequently functions to reduce its lattice energy and further decreases the viscosity of the ionic liquid, which is the reason for the superior conductivity obtained from the EMI-FSA-based ionic liquid electrolyte. [15,30].

Figure 2 displays Raman spectra of red-phosphorus powders before and after mechanical milling (MM) treatment for 10 h. The peaks located at 360, 434, and 461 cm^{-1} in the spectrum of the milled phosphorus are attributed to vibrations of crystalline lattice of black-phosphorus such as A_{1g}, B_{2g}, and A_{2g} phonon modes [31]. Furthermore, the black-phosphorus phase (Inorganic Crystal Structure Database, ICSD No. 01-073-1358) was detected in the milled red-phosphorus powder. Based on these results, it was clear that the target material was successfully synthesized. In addition, comparing the colors of these powders before and after the MM treatment, we visually confirmed that the red-phosphorus had been transformed into black-phosphorus. We employed the black-phosphorus as an active material powder because its activity against Na is higher than that of red-phosphorus.

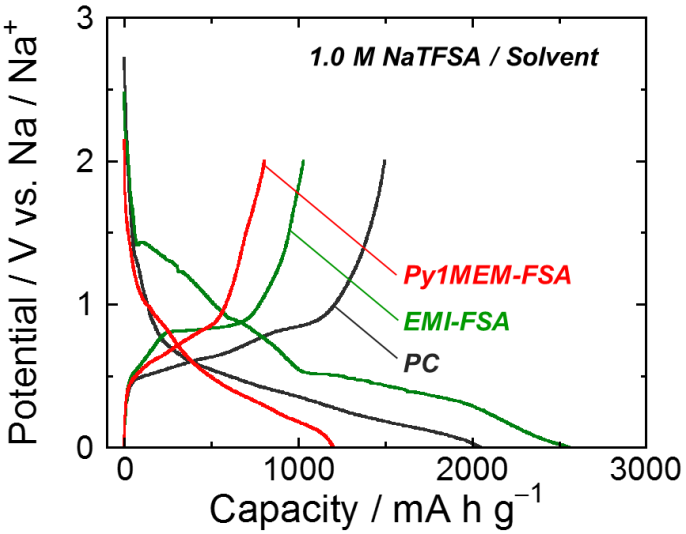

Figure 3. Charge-discharge (Na insertion-extraction) curves of black-phosphorus thick-film electrodes in 1.0 M NaTFSA-dissolved in EMI-FSA or Py1MEM-FSA. For comparison, a profile in PC is also shown. Current density: 50 mA g^{-1}.

Figure 3 shows initial charge−discharge (Na insertion−extraction) profiles of the phosphorus thick-film electrodes in 1.0 M NaTFSA-dissolved in Py1MEM-FSA or EMI-FSA. For comparison, a profile in an organic electrolyte of 1.0 M NaTFSA/PC is also shown. Among the three kinds of electrolytes, the largest discharge capacity of 1500 mA h g^{-1} was obtained when using PC. For the ionic liquid electrolytes, the capacities in Py1MEM-FSA and EMI-FSA were 800 mA h g^{-1} and 1030 mA h g^{-1}, respectively. The main reason for the relatively lower capacities in these ionic liquid electrolytes results from the strong electrostatic interaction between Na ion and FSA anions in the

ionic liquid electrolytes. Since ionic liquids do not contain any neutral molecules, in the FSA-based ionic liquid electrolyte, Na ion is inevitably solvated by several FSA anions to form $[Na(FSA)_x]^{1-x}$ complex in which "*x*" is defined as a solvation number. With respect to ionic liquid electrolytes containing bis(trifluoromethanesulfonyl)amide (TFSA) anion, Monti *et al*. demonstrated that Na ion is solvated by three TFSA anions through oxygen atoms with two bindentate and one monodentate coordination [32]. Although the solvation number of the FSA anions per Na ion is not still clear, there is no doubt that the interaction between Na ion and FSA anions is much greater than that between Na ion and neutral molecules such as PC solvent. The electrostatic interaction impedes Na-insertion into a negative electrode, and as a result, the reversible capacity decreases compared to that in an organic electrolyte system with the exception of a high-temperature operation [33]. The slightly-higher reversible capacity obtained in EMI-FSA than Py1MEM-FSA originates from its higher ionic conductivity. EMI-FSA, however, delivered an extremely low coulombic efficiency of 40% at the first cycle. In the potential range from 1.43 V to 0.53 V vs. Na/Na^+ during the charge curve, we confirmed a shoulder associated with the irreversible decomposition of the EMI cation and/or the FSA anion. Due to the high activity of the hydrogen atom at the C2 position of the EMI cation, it is considered that EMI-FSA irreversibly underwent the reductive decomposition at a relatively high potential [34]. The large polarization observed in its discharge curve probably means that the Na-ion conduction through a surface layer induced by the decomposition of EMI-FSA was hard.

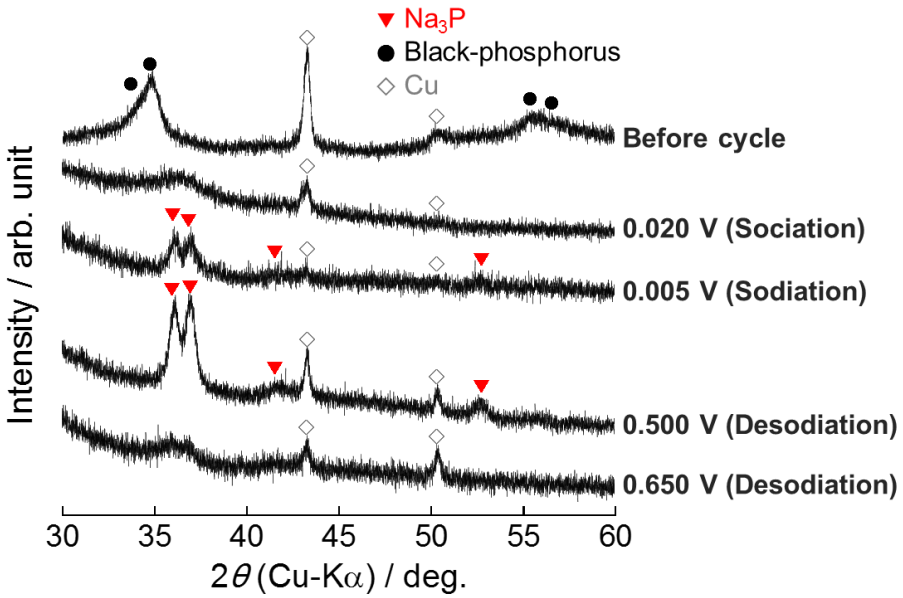

Figure 4. Ex-situ XRD patterns of phosphorus electrodes during the first charge−discharge cycle.

To investigate the reaction mechanism of phosphorus with Na during charge and discharge, we performed *ex-situ* XRD measurements at each potential using a slurry electrode composed of black phosphorus powder (70 wt.%), acetylene carbon black (10 wt.%), and polyvinyl-alcohol binder (20

wt.%). Figure 4 compares *ex-situ* XRD patterns of the phosphorus electrodes at various potentials vs. Na/Na^+. When the phosphorus electrode was electrochemically reduced to 0.200 V vs. Na/Na^+, peaks attributed to the black phosphorus disappeared, and a shoulder indicating the sodiation of phosphorus was detected at around 36.4°. Subsequently, peaks appeared at 36.1°, 37.0° and 52.7° in the fully sodiated state at 0.005 V. These peaks are attributed to the formation of hexagonal Na_3P (ICSD No. 01-073-3917). Intermediate phases, such as NaP and Na_2P, were not confirmed. This is probably because these intermediate alloy phases are amorphous as reported by other researchers [3,4]. During the electrochemical oxidation process, at the potential of 0.500 V, peaks corresponding the Na_3P phase still remained, which agrees with the charge−discharge profile obtained from the electrochemical tests. No obvious peak showing Na−P phases was confirmed at 0.65 V. In addition to this, no diffraction pattern of black phosphorus was observed after the fully desodiated state at 2.000 V (not shown here), which also indicates that phosphorus undergoes amorphization by the sodiation and desodiation processes. Based on the *ex-situ* XRD analysis, phosphorus appears to react with Na as shown in the following equations:

$$P + xNa^+ + xe^- \rightleftarrows Na_xP \qquad (1)$$

$$Na_xP + yNa^+ + ye^- \rightleftarrows Na_3P \qquad (2)$$

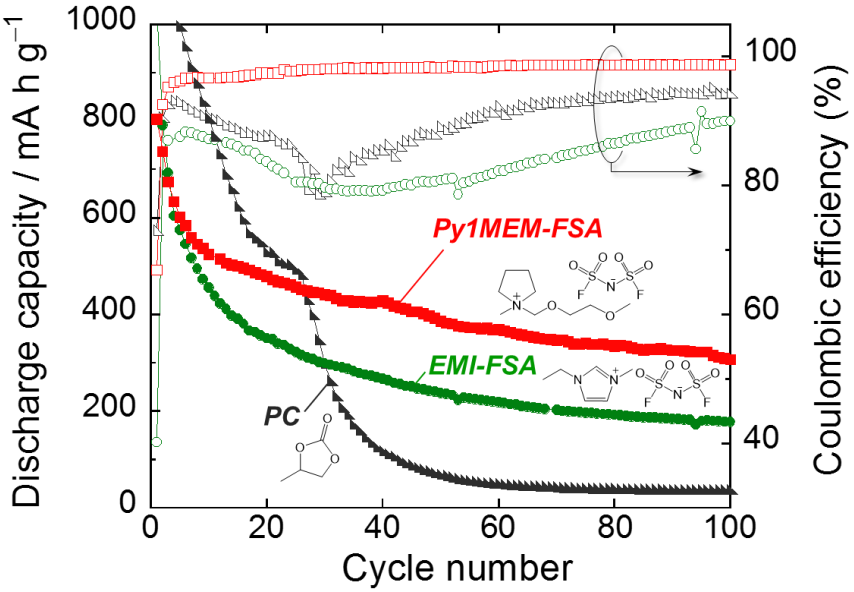

Figure 5. Dependence of discharge (Na-extraction) capacities and coulombic efficiencies on cycle number for black-phosphorus electrodes in various electrolytes. The initial discharge capacities in PC and EMI-FSA were 1500 and 1030 mA h g^{-1}, respectively.

Figure 5 represents dependence of discharge (Na-extraction) capacities and coulombic efficiencies of the phosphorus electrodes in the ionic liquid and the organic electrolytes. Although the phosphorus electrode in PC showed the high discharge capacity of 1500 mA h g^{-1} for the first cycle,

the capacity quickly decreased to 110 mA h g^{-1} by the 40th cycle, and thus resulted in a very poor cycling performance. The volume change ratio from P to Na_3P phase is 490%, which is responsible for the generation of high stresses causing large strains in the active material [3,4]. The accumulated strains by repeated charge−discharge cycling lead to the disintegration of an electrode. In the PC-based electrolyte, we could confirm noticeable changes in surface morphology of the phosphorus electrode and the resulting exposed Cu foil (Figure 6).

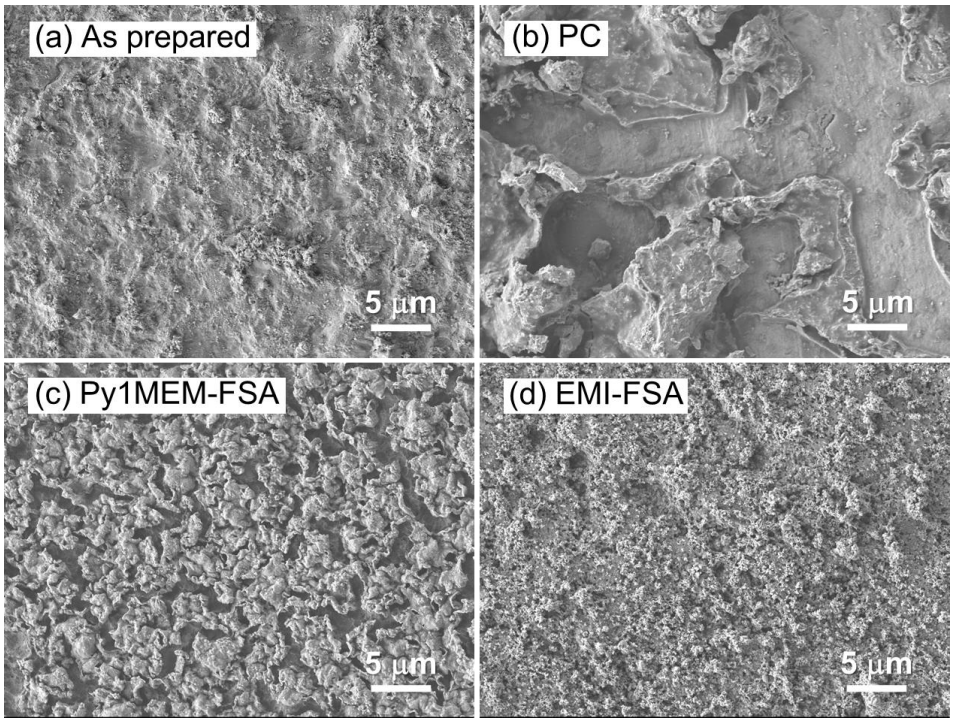

Figure 6. FE-SEM images of phosphorus electrodes (a) as prepared and after charge−discharge cycling in (b) PC, (c) Py1MEM-FSA, and (d) EMI-FSA.

Organic electrolytes are generally decomposed during charge process to form a surface layer on a negative electrode. The decline in the coulombic efficiency during the initial 30th cycle in PC implies the continuous electrolyte decomposition which took place along with the disintegration of the phosphorus electrode [3]. The continuous growth of surface layer increases the resistance for Na-insertion into the phosphorus, and it reduces the reversibility and the activity for sodiation/desodiation reactions of phosphorus. We controlled the volumetric changes in phosphorus during charge−discharge cycling tests by adjusting the amount of Na insertion−extraction with a constant capacity of 500 mA h g^{-1} (Figure 7), which suggests that a long cycle lifetime can be successfully achieved. Contrary to our expectation, the capacity was maintained only up to the 10th cycle, and then the capacity gradually dropped down. This result reflects that the decomposition products of the electrolyte passivated surface parts of the electrode, and thereby reduced utilization of the active material. It is inferred that the reason for the capacity decay in PC lies not only in the disintegration, but also the passivation by the surface layer on the phosphorus electrode. In contrast to the organic electrolyte system, Py1MEM-FSA

delivered a superior cycle performance; a relatively high discharge capacity of 310 mA h g^{-1} was attained at the 100th cycle. Compared with surface morphology of both phosphorus electrodes after charge−discharge cycling (Figures 6b and 6c), it is obvious that, in Py1MEM-FSA, the disintegration of the electrode was significantly suppressed.

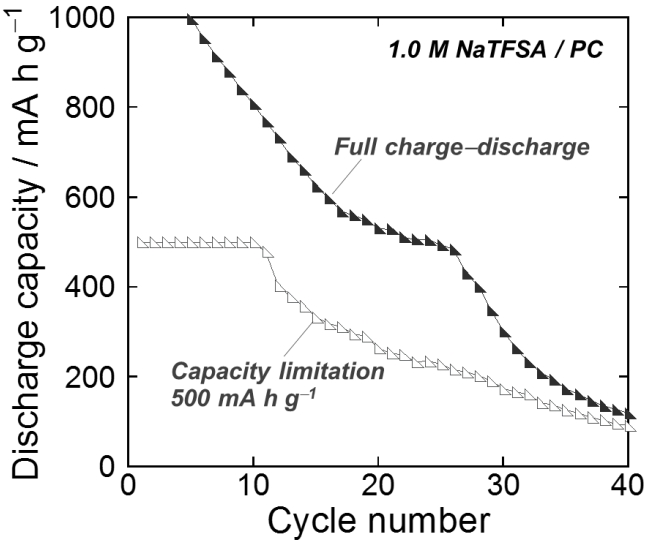

Figure 7. Variation in discharge (Na-extraction) capacity of phosphorus electrodes in 1.0 M NaTFSA-dissolved in PC versus cycle number for Na-insertion level fixed to 500 mA h g^{-1}. For comparison, performance without capacity limit is also plotted.

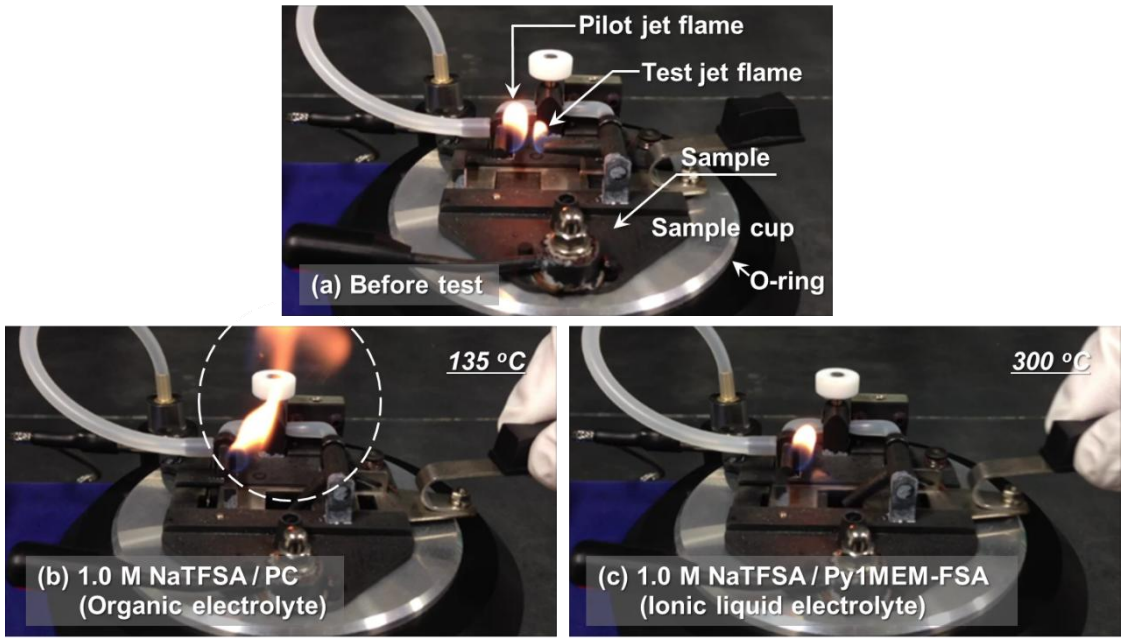

Figure 8. (a) Photographs of fire-resistance tester (Setaflash Series: 33000-0). Fire-resistance tests of (b) 1.0 M NaTFSA/PC (organic electrolyte) and (c) 1.0 M NaTFSA/Py1MEM-FSA (ionic liquid electrolyte).

Furthermore, the regions in which the disintegration occurred were not localized, but were generated over the entire electrode in comparison that in PC. The most noteworthy point is that surface morphologies markedly varied by an electrolyte solvent. In studies of the Li-ion battery, we previously found that Li-ions are uniformly inserted into a Si electrode over the entire surface by an ionic-liquid-derived surface layer [23]. The Si electrode can reasonably avoid stress accumulation generated in localized regions, which suppresses the severe disintegration of the electrode leading to a poor cycling performance. From the SEM observations, we considered that the mechanism of the improved performance of the Si electrode is just as valid for the phosphorus electrode in Py1MEM-FSA, that is, the Py1MEM-FSA-derived surface layer allowed uniform Na-insertion into the phosphorus electrode. On the other hand, in EMI-FSA, the discharge capacity gradually decreased and was 180 mA h g^{-1} at the 100th cycle though the capacity was higher than that in PC. The coulombic efficiency in Py1MEM-FSA reached a value exceeding 95% after the second cycle, whereas the efficiency in EMI-FSA constantly remained below 90% throughout every cycle. This phenomenon means a side reaction such as continuous growth of a surface layer induced by the decomposition of EMI-FSA, which is the cause of the increase in the resistance for the interfacial Na-ion transfer between phosphorus electrode and EMI-FSA. Since the degree of change in the electrode surface after cycling in EMI-FSA was actually smaller than that in Py1MEM-FSA (Figure 6d), it is considered that the deterioration of the electrode arose from a decrease in utilization of the active material due to the surface layer formed on the anode. We will investigate the characteristics of the surface layers such as the chemical composition and thickness in a future study. Experimental results show that the selection of cation in ionic liquids has a significant influence on the cycle performance of a phosphorus electrode, and indicated that ionic liquids with cations having a high stability against cathodic decomposition are needed for achieving a long life cycle.

Figure 8 shows fire resistance test results of the electrolytes employed in this study. Conventionally, the flammability of ionic liquid electrolytes has been examined by directly exposing its solution to a test flame at room temperature [35]. Although this test is a simplified evaluation method to easily understand, the vapor of its solution generated by the heat hardly reaches its combustion limitation because of an open-type measurement, and thereby results in an overestimation. On the other hand, the closed-system evaluation method (Rapid equilibrium closed cup method) [27,28] used in this study is prescribed by IOS-standard and JIS. The flame retardant property can therefore be evaluated with a good accuracy and reproducibility. We, the first time, introduced this technique as the evaluation method for the flame retardancy of ionic liquid electrolytes. When using the organic electrolyte of 1.0 M NaTFSA/PC, the electrolyte ignited with a large flame at the relatively low temperature of 135 ^{o}C (Figure 8b). In contrast, no fire was observed at 300 ^{o}C (measurement limitation) in the ionic liquid electrolyte of 1.0 M NaTFSA/Py1MEM-FSA (Figure 8c), which clearly demonstrates the non-flammability of the ionic liquid. This characteristic contributes to the establishment of highly safe Na-ion batteries, and allows the charge−discharge reactions over a wide temperature range.

Figure 9 exhibits a rate performance of the phosphorus electrode in Py1MEM-FSA at 60 ^{o}C. Although the reversible capacity decreased with the increasing current density, the capacity of 1380 mA h g^{-1} was achieved at a current density of 50 mA g^{-1}, and the capacity was 1.7 times larger than

that obtained at 30 °C. This is because the ionic transport property, kinetics of the desolvation of $[Na(FSA)_x]^{1-x}$, and solid-phase diffusion were improved. The significant enhancement was confirmed only in Py1MEM-FSA, and the charge−discharge capacities in PC became small. This is considered to be due to the poor thermal stability of the electrolyte solvent itself and a surface layer formed on the anode [36].

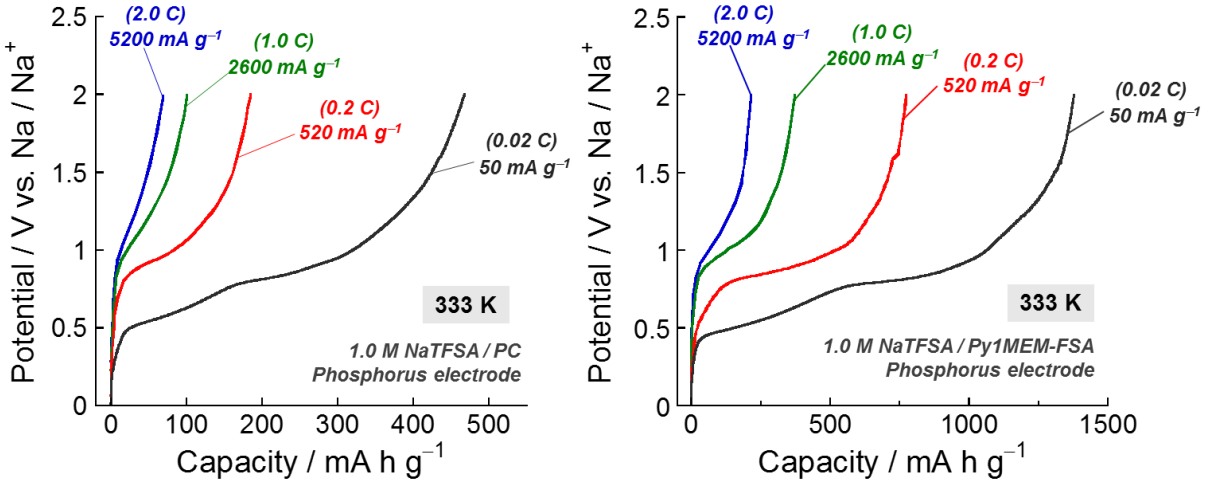

Figure 9. Rate capability of phosphorus electrode in (a) 1.0 M NaTFSA/PC and (b) 1 M NaTFSA/Py1MEM-FSA at 333 K. Rapid charge-discharge property was evaluated at various current densities from 50 (0.02 *C*) to 5200 mA g^{-1} (2.0 *C*).

4. CONCLUSION

Black phosphorus powder was simply synthesized by mechanical milling, and phosphorus electrodes without any binder or conductive additive were prepared by a gas-deposition method using the resulting powder. For the first time, we investigated the applicability of ionic liquid electrolytes using a phosphorus electrode as the Na-ion battery anode. The phosphorus electrode in Py1MEM-FSA exhibited the best cycling performance. The discharge capacity at the 100th cycle was 310 mA h g^{-1} with a capacity retention of approximately 40%. The good electrode property is based on its high stability against cathodic decomposition. On the other hand, an organic electrolyte, 1.0 M NaTFSA-dissolved in PC, delivered the poor cycling performance; the capacity decreased to 40 mA h g^{-1} by the 100th cycle though the electrode showed the initial high capacity of 1500 mA h g^{-1}. Based on the SEM observation results, it was revealed that the use of Py1MEM-FSA allowed the uniform Na-insertion into the phosphorus electrode surface, which avoids the disintegration of the electrode leading to a poor electrode property. In light of the low-electrochemical stability of EMI-FSA and the smallest degree of change in the electrode surface after cycling, the reason for the capacity decay in EMI-FSA is that the surface layer induced by the irreversible decomposition of it restricts Na-insertion into the electrode. In the cycling test at a relatively high temperature of 60 °C, the charge−discharge capacities were significantly increased only in Py1MEM-FSA which showed an excellent fire resistance. This

property indicates that the application of the ionic liquid as an electrolyte solvent is an advantage for realizing a Na-ion battery combining a high energy density and a high safety.

ACKNOWLEDGMENTS
This work was supported in part by the Adaptable and Seamless Technology Transfer Program through target-driven R&D funding from the Japan Science and Technology Agency (JST). M. Shimizu thanks Japan Society for the Promotion of Science (JSPS) for research fellowship (No. 2611485). The authors appreciate Dr. H. Furutani (KANEKA Co., Japan) and Mr. K. Matsumoto for supplying chemicals and synthesis of ionic liquids, respectively.

References

1. S. Komaba, W. Murata, T. Ishikawa, N. Yabuuchi, T. Ozeki, T. Nakayama, A. Ogata, K. Gotoh, K. Fujiwara, *Adv. Funct. Mater*., 21 (2011) 3859.
2. M. Dahbi, N. Yabuuchi, K. Kubota, K. Tokiwa, S. Komaba, *Phys. Chem. Chem. Phys*., 16 (2014) 15007.
3. J. Qian, X. Wu, Y. Cao, X. Ai, H. Yang, *Angew. Chem*., 52 (2013) 4633.
4. Y. Kim, Y. Park, A. Choi, N.S. Choi, J. Kim, J. Lee, J.H. Ryu, S.M. Oh, K.T. Lee, *Adv. Mater*., 25 (2013) 3045.
5. W.J. Li, S.L. Chou, J.Z. Wang, H.K. Liu, S.X. Dou, *Nano Lett*., 13 (2013) 5480.
6. Y. Cao, L. Xiao, M.L. Sushko, W. Wang, B. Schwenzer, J. Xiao, Z. Nie, L.V. Saraf, Z. Yang, J. Liu, *Nano Lett*., 12 (2012) 3783.
7. T. Matsushita, Y. Ishii, S. Kawasaki, *Mater. Express*, 3 (2013) 30.
8. A. Ponrouch, A.R. Goñi, M.R. Palacín, *Electrochem. Commun*., 27 (2013) 85.
9. M.K. Datta, R. Epur, P. Saha, K. Kadakia, S.K. Park, P.N. Kumta, *J. Power Sources*, 225 (2013) 316.
10. T. Yamamoto, T. Nohira, R. Hagiwara, A. Fukunaga, S. Sakai, K. Nitta, S. Inazawa, *J. Power Sources*, 217 (2012) 479.
11. J. Qian, Y. Chen, L. Wu, Y. Cao, X. Ai, H. Yang, *Chem. Commun*., 48 (2012) 7070.
12. A. Darwiche, C. Marino, M.T. Sougrati, B. Fraisse, L. Stievano, L. Monconduit, *J. Am. Chem. Soc*., 134 (2012) 20805.
13. Q. Sun, Q.-Q. Ren, H. Li, Z.-W. Fu, *Electrochem. Commun.*, 13 (2011) 1462.
14. L.D. Ellis, B.N. Wilkes, T.D. Hatchard, M.N. Obrovac, *J. Electrochem. Soc*., 161 (2014) A416.
15. M. Yamagata, N. Nishigaki, S. Nishishita, Y. Matsui, T. Sugimoto, M. Kikuta, T. Higashizaki, M. Kono, M. Ishikawa, *Electrochim. Acta*, 110 (2013) 181.
16. J. Kosters, M. Schonhoff, N.A. Stolwijk, *J. Phys. Chem. B*, 117 (2013) 2527.
17. K. Kubota, T. Nohira, R. Hagiwara, *Electrochimica Acta*, 66 (2012) 320.
18. K. Tsunashima, M. Sugiya, *Electrochem. Commun*., 9 (2007) 2353.
19. L. Lombardo, S. Brutti, M.A. Navarra, S. Panero, P. Reale, *J. Power Sources*, 227 (2013) 8.
20. H. Usui, T. Masuda, H. Sakaguchi, *Chem. Lett*., 41 (2012) 521.
21. H. Usui, M. Shimizu, H. Sakaguchi, *J. Power Sources*, 235 (2013) 29.
22. M. Shimizu, H. Usui, K. Matsumoto, T. Nokami, T. Itoh, H. Sakaguchi, *J. Electrochem. Soc*., 161 (2014) A1765.
23. M. Shimizu, H. Usui, T. Suzumura, H. Sakaguchi, *J. Phys. Chem. C*, 119 (2015) 2975.
24. H. Sakaguchi, T. Toda, Y. Nagao, T. Esaka, *Electrochem. Solid-State Lett*., 10 (2007) J146.
25. H. Usui, Y. Kiri, H. Sakaguchi, *Thin Solid Films*, 520 (2012) 7006.
26. T. Nokami, K. Matsumoto, T. Itoh, Y. Fukaya, T. Itoh, *Org. Process Res. Dev*., 18 (2014) 1367.
27. ISO 3679:2004, https://www.iso.org/obp/ui/#iso:std:iso:3679:ed-3:v1:en, (accessed April 2015).

28. JISK2265-2, http://www.jisc.go.jp/app/pager?id=538998, (accessed April 2015).
29. M. Shimizu, H. Usui, H. Sakaguchi, *J. Power Sources*, 248 (2014) 378.
30. H. Matsumoto, H. Sakaebe, K. Tatsumi, M. Kikuta, E. Ishiko, M. Kono, *J. Power Sources*, 160 (2006) 1308.
31. C. A. Vanderborgh, D. Schiferl, *Phys. Rev. B*, 40 (1989) 9595.
32. D. Monti, E. Jónsson, M.R. Palacín, P. Johansson, *J. Power Sources*, 245 (2014) 630.
33. A. Fukunaga, T. Nohira, R. Hagiwara, K. Numata, E. Itani, S. Sakai, K. Nitta, S. Inazawa, *J. Power Sources*, 246 (2014) 387.
34. M.C. Buzzeo, R.G. Evans, R.G. Compton, *ChemPhysChem*, 5 (2004) 1106.
35. N. Wongittharom, C.H. Wang, Y.C. Wang, C.H. Yang, J.K. Chang, *ACS Appl. Mater. Interfaces*, 6 (2014) 17564.
36. A. Ponrouch, E. Marchante, M. Courty, J.-M. Tarascon, M.R. Palacín, *Energy Environ. Sci.*, 5 (2012) 8572.